Automated Brain Tissue Assessment in the Elderly and Demented Population: Construction and Validation of a Sub-Volume Probabilistic Brain Atlas

Michael S. Mega, M.D., Ph.D. (1), Ivo I. Dinov, Ph.D. (2), Paul Thompson. Ph.D. (3), Mario Manese, M.S. (4), Chris Lindshield, M.D. (5), Jacob Moussai, M.D. (6), Nah Tran, B.S. (7), Kirsten Olsen, M.D. (8), Jenaro Felix, M.A. (9), Chris I. Zoumalan, M.D. (10), Roger P. Woods, M.D. (11), Arthur W. Toga, Ph. D. (12), John C. Mazziotta, M.D., Ph.D. (13)

Key Words: Alzheimer's disease, MRI, Brain Mapping, Neuro Imaging

From the Laboratory of Neuro Imaging (1-13), and Division of Brain Mapping (11-13), Department of Neurology (1-13), and Department of Statistics (2), UCLA School of Medicine, Los Angeles, California, USA.

Address correspondence to: Michael S. Mega, M.D., Ph.D.
Neural Net Research
5910 SW Ralston Drive
Portland, OR 97239, USA
Telephone (503) 892-2498
email mega@neural-net.org

Introduction

Neuroimaging in aging and dementia is now at a critical turning point. The accumulation of findings since the first functional and structural studies of dementia has produced sufficient observational data to bring the field to the threshold of a new challenge—the identification of incipient Alzheimer's disease in the individual. Results from past observational studies in patients, and elderly normal subjects, enable us to test the *prospective* sensitivity and specificity of a few discrete regional abnormalities in correctly identifying incipient AD. Unfortunately, no single institution can easily amass enough longitudinal population data to power the analysis of an individuals' likelihood of having incipient AD. The urgency in meeting the challenge of identifying the individual, who may not even have cognitive complaints, prior to developing dementia symptoms is now apparent given our society's changing demographics and the emergence of disease modifying treatments. A major impediment to meeting this challenge is the development of an imaging strategy that can be universally applied and possess sufficient power to identify an individual's disease risk compared to an unaffected population.

Four difficulties face the development of this imaging strategy: 1) The imaging strategy must control for anatomic variability and registration errors produced when comparing datasets in a common co-ordinate system; 2) The imaging strategy must allow for regionally testable hypotheses; 3) To ensure inter-center application the imaging strategy must be automated, freely available, and not require extensive computer resources; and 4) The imaging analysis should accommodate growth in its population data. This study demonstrates a candidate imaging strategy that addresses the above difficulties.

Methods

Overview. To determine the best registration algorithm to a common target space (a population based Atlas designed to accommodate the elderly and demented brain previously described)[1] we test three registration approaches to our Atlas target using Automated Image Registration (AIR):[2] 12 parameter affine (12p), 30 parameter 2nd order warp (2nd order), or 168 parameter 6th order warp (6th order) using 3 dimensional magnetic resonance imaging (3-D MRI) data in 20 subjects. Regional native space tissue counts derived from manual outlines serve as the gold standard to determine the best overall accuracy of automated grey matter (GM), white matter (WM), and cerebral spinal fluid (CSF) counts derived from the three registration approaches. Regional sub-volume probability gradients produced within the Atlas target space from the three registration approaches are constructed by projecting the manual outlines down the three registration matrices. Thus, three sub-volume probabilistic Atlas (SVPA) models are constructed for use as automated tissue counters. The counts obtained with these three SVPA's are then compared to the manual "gold standard" counts to determine the best SVPA model.

Subjects. The study group consisted of 20 individuals who presented to the University of California Los Angeles (UCLA) Alzheimer's Disease Research Center, met all study criteria (below), and agreed to scanning after signing an informed consent approved by the Human Subjects Protection Committee. This study included 6 patients with moderate Alzheimer's Disease (AD), and 7 patients with mild disease all diagnosed according to National Institute of Neurological and Communicative Disorders and Stroke/Alzheimer's Disease and Related Disorders Association (NINCDS/ADRDA) criteria for probable AD,[3] 4 patients with Mild Cognitive Impairment (MCI) meeting criteria described by Petersen et al,[4] and 3 normal elderly subjects enrolled from a population of patient caregivers. We chose a distribution of mild to

moderate AD patients, and MCI and controls to extend the application of the SVPA across the population spectrum seen in most clinical research settings. Inclusion criteria included no history of psychiatric in all subjects, or non-AD neurological illness in the AD patients, being sufficiently proficient in English to perform clinical evaluation and age 60 or greater. Exclusion criteria included: all individuals with an abnormal structural imaging study of the brain, a current or recent psychiatric illness (i.e. manic depressive states, schizophrenia); significant, uncontrolled systemic illness (i.e. chronic renal failure, chronic liver disease, poorly controlled diabetes, or poorly controlled congestive heart failure); a history of alcoholism or substance abuse within the past year. Severity of the cognitive deficit was measured in all subjects using the Mini Mental State Exam (MMSE)[5] revealed an average score for the group of 23 (SD 5.39); moderate AD patients scored between 15-19 with mild patient scoring between 20-25. There were a total of 9 females and 11 males, an average age of 76.1 (SD 6.36), and average educational level of 15.6 (SD 2.75).

Scanning Protocol. All scans were derived from a GE 1.5T scanner with the following protocol: Coronal 3D volumetric spoiled gradient echo, flip angle 25, TE=minimum FULL, TR=minimum, FOV= 22 cm x 16.5 cm, 124 slices at 1.6 mm/slice, matrix 256 x192, phase FOV (rectangular FOV), $\pm$ 10 kHz BW.

Image Processing. All scans were transferred from archived digital sources in 16bit format and manually edited to remove the skull and scalp taking particular caution to preserve the sulcal and subdural CSF. A binary brain mask was then created from the manually edited file and used in a radio frequency bias field correction algorithm using a histogram spline sharpening method[6] to eliminate intensity drifts attributable to scanner field inhomogeneity. After inhomogeneity correction a supervised tissue classifier generated detailed maps of GM, WM,

and CSF in the subjects' native space. Briefly, 120 samples of each tissue class were interactively tagged to compute the parameters of a Gaussian mixture distribution that reflects statistical variability in the intensity of each tissue type.[7] A nearest neighbor tissue classifier assigned each image voxel to a particular tissue class (GM, WM, or CSF) or to a background class (representing extra-cerebral voxels in the image). The inter-rater and intra-rater reliability of this protocol, and its robustness to changes in image acquisition parameters, have been described previously.[8] Gray and white matter maps were retained for subsequent analysis. Native space, skull-stripped, inhomogeneity corrected images were then registered to the standard 3D stereotaxic Atlas space[1] using AIR[2] to produce three registration matrices: 12 parameter affine (12p), 30 parameter 2nd order warp (2nd order), or 168 parameter 6th order warp (6th order).

Regions of Interest (ROI) construction. To aid manual ROI construction a surface model of each subject's cortex was automatically extracted[9] as previously described.[10] A mesh-like surface is deformed to fit the brain-CSF tissue intensity value of each skull-stripped image volume. The cortical surface software was modified to permit high-resolution extraction of both the lateral and medial hemispheric surfaces, aiding ROI volumetric construction on orthogonal image slices. The following landmarks were outlined on each dataset: the Sylvian fissure; central, precentral, and postcentral sulci; superior temporal sulcus (STS) main body, STS ascending and posterior branches, and primary and secondary intermediate sulci; inferior temporal, superior and inferior frontal, intraparietal, transverse occipital, olfactory, occipitotemporal, collateral, callosal sulcus and inferior callosal boarder; the paracentral, anterior and posterior cingulate and the outer segment of double parallel cingulate sulci (when present);[11] the superior and inferior rostral, parieto-occipital, anterior and posterior calcarine, and

subparietal sulci. This protocol is available on the internet[12, 13] and has known inter-rater and intra-rater reliability, as previously reported.[14]

In addition to contouring the major and minor sulci, a set of six midline landmark curves bordering the longitudinal fissure was outlined in each hemisphere to establish limits to aid dividing the brain ROI into left and right. Spatially registered gray scale image volumes in the three orthogonal coronal, axial, and sagittal planes (available for simultaneous viewing with the 3D surface model in the Display software package run on the McIntosh OS X platform available at: http://www.bic.mni.mcgill.ca/software/Display/Display.html) were manually segmented into 34 volumetric ROI for each subject's left and right hemisphere (see Figure 1 and Table 1). All surface and deep brain landmarks were defined according to detailed anatomical protocols[11-16] and atlasing methods.[17-23] Extension of the gyral ROI into the underlying WM was accomplished by a "spokes-of-the wheel" technique with its pattern, defined in the Atlas target space, projected down 9 parameter transforms into each subject's native space data reoriented to the Atlas via rigid body transforms. In this canonical orientation each subject's brain data was manually edited to produce the landmarks and ROI described above. Once all 68 left and right 3D ROI were created the GM, WM, and CSF tissue maps were used to partition the ROI into their three tissue components. These subdivided ROI where then projected down the 3 transformation matrices into the Atlas space to construct probability maps for 12p, 2nd order, and 6th order SVPA's.

Table 1 and Figure 1

SVPA construction. **IVO PLEASE INSERT METHODS HERE FOR CONSTRUCTION AND TISSUE COUNTING IN THE SVPA's.**

SVPA validation. Determining which of the three constructed SVPA's best extracts automated tissue counts a comparison of the native space manual "gold standard" ROI counts was preformed via Pearson correlation coefficients for each of the 66 ROI in the three SVPAs's across the 20 subjects. Absolute tissue counts and tissue counts corrected for each subject's intracranial volume (IVC) were assessed. Guided from our previous experience with past SVPA construction[24] we also evaluated GM, and WM ratios (GM+CSF/CSF = GM%, and WM+CSF/CSF = WM%) since the tissue probability clouds in the automated SVPA assessments count all three tissue types and atrophy will increase the CSF component of the automated counts.

Results

Figure 2ABC demonstrates the Pearson correlation coefficients for the absolute tissue counts in the 3 SVPA's compared to the "gold standard" native space counts. Evaluation of the ICV corrected counts showed no advantage over absolute counts. Regions with the smallest tissue components (e.g. ventricular GM, and WM) have the worst automated correlations to the manually derived counts. Regional gradients constructed from higher order warps often showed superiority to the gradients derived from the linear registrations to the atlas.

Figure 2ABC

Given that the probability gradients constructed from the three tissue types will count all voxels from the GM, WM, and CSF that fall within them in any given subject the GM ratio (GM% = GM+CSF/CSF) and WM ratio (WM% = WM+CSF/CSF) counts were also compared to the manually derived ratios as shown in Figure 3AB. Absolute counts were used instead of

ratio counts in Figure 3AB however when the regions had primarily one tissue type (absolute CSF counts used for the ventricles in A and B, absolute GM counts used for the hippocampus, thalamus, subtantia nigra, lenticular, and caudate nuclei in A). The use of ratios markedly improved the correlation in the automated counting methods compared to manual counting across most regions with the mean left and right GM ratio "r values" for the 3 SVPAs being 0.87 for the 12p SVPA, 0.895 for the 2nd SVPA, and 0.90 for the 6th SVPA (calculated with the absolute GM substitutions noted above).

Figure 3AB

Visual inspection of the probability gradients constructed from the three different registration matrices reveals the population's anatomical variability, and how that variability is controlled across high parameter and low parameter registrations as shown for the medial temporal regions in Figure 4ABC. Right-sided variability of the amygdala and hippocampus is controlled better with 6th order warps compared to 12 parameter linear registrations (also see Figure 3A for "r values" derived in the ratio counts from these regional gradients).

Figure 4ABC

The most difficult region for the automated SVPA to control population variability in was the parahippocampus (see Figures 5ABC and Figure 3A). Although high order warping improved GM ratio counts in the 6th order SVPA over the 2nd order and 12 parameter SVPAs for the right anterior parahippocampus it did not improve these counts in the left posterior parahippocampus.

Figure 5ABC

Control of cortical variability by high order warping was best in the left lateral orbitofrontal cortex as seen in Figure 6A. In addition to medial temporal laterality differences across the three SVPAs' performance in automated tissue counting the sub-callosal medial frontal area was another paralimbic region having marked asymmetry in variability (see Figure 6B and Figure 3A).

Discussion

We sought to develop an imaging assessment method that achieved the following goals: 1) The imaging strategy must control for anatomic variability and registration errors produced when comparing datasets in a common coordinate system. We chose a Talairach compatible coordinate system constructed from a population most similar to that found in clinics evaluating dementia patients as our "target atlas space".[1, 10, 25, 26] The best SVPA within this atlas space is somewhat regionally dependent but in general the higher order 2nd and 6th SVPAs out performed the 12p SVPA in controlling anatomic variability and registration errors. The increased processing time necessary for the higher order warps (30 min. versus 5 min. when run on a G4 processor on the McIntosh OSX platform) might out weigh the 3% improvement in accuracy (average r = 0.90 for 6th SVPA versus 0.87 for the 12p SVPA).

2) The imaging strategy must allow for regionally testable hypotheses. This is the first imaging assessment technique that allows for such diverse regionally selected brain analysis given the 204 sub-volumes embedded in each SVPA. 3) To ensure inter-center application the imaging strategy must be automated, freely available, and not require extensive computer

resources. We present here an automated tissue counting method that uses freely available software packages compiled on a G4 McIntosh running OSX. 4) The imaging analysis should accommodate growth in its population data. Use of this assessment method will provide regional tissue counts for an individual subject with the standard deviation each count has within a larger population. This population will increase in size as the number of subjects measured by it increases. The population distribution data will be made available to the users of this method contingent upon their sharing of their data with other users. Only through open sharing of the assessment technique and growing population can sufficient statistical power be achieved to diagnosis disease in individual patients.

References

1. Thompson PM, Mega MS, Woods RP, et al. Cortical change in Alzheimer's disease detected with a disease-specific population-based brain atlas. Cerebral Cortex 2001;11:1-16.

2. Woods RP, Grafton ST, Watson JDG, Sicotte NL, Mazziotta JC. Automated image registration: II. Intersubject validation of linear and nonlinear models. J Comput Assist Tomogr 1998;22:153-165.

3. McKhann G, Drachman D, Folstein M, Katzman R, Price D, Stadlan EM. Clinical diagnosis of Alzheimer's disease: report of the NINCDS-ADRDA Work Group, Department of Health and Human Services Task Force on Alzheimer's Disease. Neurology 1984;34:939-944.

4. Petersen RC, Smith GE, Waring SC, Ivnik RJ, Tangalos EG, Kokmen E. Mild cognitive impairment: clinical characterization and outcome. Arch Neurol 1999;56:303-308.

5. Folstein MF, Folstein SE, McHugh PR. "Mini-mental state": A practical method for grading the mental state of patients for the clinician. J Psychiatry Res 1975;12:189-198.

6. Sled JG, Zijdenbos AP, Evans AC. A nonparametric method for automatic correction of intensity nonuniformity in MRI data. IEEE Trans Med Imag 1998;17:87-97.

7. Zijdenbos AP, Dawant BM. Brain segmentation and white matter lesion detection in MR images. Crit Rev Biomed Eng 1994;22:401-465.

8. Sowell ER, Thompson PM, Holmes CJ, Jernigan TL, Toga AW. Progression of structural changes in the human brain during the first three decades of life: in vivo evidence for post-adolescent frontal and striatal maturation. Nat Neurosci 1999;2:859-861.

9. MacDonald D, Kabani N, Avis D, Evans AC. Automated 3-D extraction of inner and outer surfaces of cerebral cortex from MRI. NeuroImage 2000;12:340-356.

10. Thompson PM, Mega MS, Vidal C, Rapoport JL, Toga AW. Detecting disease-specific patterns of brain structure using cortical pattern matching and a population-based probabilistic brain atlas. In: Insana M, Leahy R, ed. IEEE Conference on Information Processing in Medical Imaging. Davis, CA: New York: Springer, 2001: 488-501.

11. Ono M, Kubik S, Abernathey CD. Atlas of the cerebral sulci.Stuttgart: Georg Thieme Verlag, 1990

12. Sowell ER, Thompson PM, Mega MS, Zoumalan CI, Lindshield C, Rex DE. Gyral pattern delineation in 3D: surface curve protocol (http://www.loni.ucla.edu/esowell/new_sulcvar.html). 2000

13. Hayashi KM, Thompson PM, Mega MS, Zoumalan CI. Medial hemispheric surface gyral pattern delineation in 3D: surface curve protocol (http://www.loni.ucla.edu/khayashi/Public/medial_surface/MedialLinesProtocol). In: 2002:

14. Sowell ER, Thompson PM, Tessner KD, Toga AW. Accelerated brain growth and cortical gray matter thinning are inversely related during post-adolescent frontal lobe maturation. J Neurosci 2001;21:8819-8829.

15. Steinmetz H, Furst G, Freund H-J. Variation of perisylvian and calcarine anatomic landmarks within stereotaxic proportional coordinates. Am J Neuroradiol 1990;11:1123-1130.

16. Leonard CM. Structural variation in the developing and mature cerebral cortex: noise or signal? In: Thatcher RW, Reid LG, Rumsey J, Krasnegor N, ed. Developmental neuroimaging: mapping the development of brain and behavior. New York: Academic Press, 1996: 207–231.

17. Kim J-J, Crespo-Facorro B, Andreasen NC, et al. An MRI-Based Parcellation Method for the Temporal Lobe. NeuroImage 2000;11:271-288.

18. Chiavaras MM, LeGoualher G, Evans AC, Petrides M. Three-Dimensional Probabilistic Atlas of the Human Orbitofrontal Sulci in Standardized Stereotaxic Space. NeuroImage 2001;13:479-496.

19. Amunts K, Malikovic A, Mohlberg H, Schormann T, Zilles K. Brodmann's Areas 17 and 18 Brought into Stereotaxic Space—Where and How Variable? NeuroImage 2000;11:66-84.

20. Crespo-Facorro B, Kim J-J, Andreasen NC, et al. Human Frontal Cortex: An MRI-Based Parcellation Method. NeuroImage 1999;10:500-519.

21. Geyer S, Schormann T, Mohlberg H, Zilles K. Areas 3a, 3b, and 1 of Human Primary Somatosensory Cortex2. Spatial Normalization to Standard Anatomical Space. NeuroImage 2000;11:684-696.

22. Sastre-Janer FA, Regis J, Belin P, et al. Three-Dimensional Reconstruction of the Human Central Sulcus Reveals a Morphological Correlate of the Hand Area. Cerebral Cortex 1998;8:641-647.

23. White LE, Andrews TJ, Hulette C, et al. Structure of the Human Sensorimotor System. I: Morphology and Cytoarchitecture of the Central Sulcus. Cerebral Cortex 1997;7:18-30.

24. Mega MS, Thompson PM, Cummings JL, Toga AW. The UCLA Alzheimer's disease atlas project: Structural and functional applications. Ann Neurol 2000;48:427.

25. Thompson PM, Woods RP, Mega MS, Toga AW. Mathematical and computational challenges in creating deformable and probabilistic atlases of the human brain. Human Brain Mapping 2000;9:81-92.

26. Thompson PM, Mega MS, Toga AW. Disease-specific probabilistic brain atlases. In: IEEE, ed. Proceedings of the International Conference on Computer Vision and Pattern Recognition, and Workshop on Mathematical Methods in Biomedical Image Analysis. 2000: 237-234.

Table 1. Regions constructed in the three sub-volume probabilistic atlases (SVPA's) associated with their numerical labels shown in the Pearson correlation graphs in Figures 2 and 3. Each region has probability gradients constructed from the three tissue types derived from the segmentation of native space scans of 20 subjects registered to the atlas across three matrices.

Region	Label
Cerebellum	1
Occipital	2
Superior Parietal	3
Inferior Parietal	4
Posterior Cingulate	5
Superior Temporal	6
Middle Temporal	7
Inferior Temporal	8
Anterior Parahippocampal	9
Hippocampus	10
Amygdala	11
Temporal Pole	12
Posterior Parahippocampal	13
Caudal Anterior Cingulate	14
Rostral Anterior Cingulate	15
Sub-Callosal Frontal	16
Medial Orbital Frontal	17
Lateral Orbital Frontal	18
Inferior Frontal	19
Middle Frontal	20
Superior Frontal	21
Pre-Central	22
Post-Central	23
Insula	24
Ventricles	25
Substantia Nigra	26
Midbrain	27
Pons	28
Medulla	29
Basal Medial Diencephalon	30
Thalamus	31
Nucleus Accumbens	32
Lenticular Nucleus	33
Caudate Nucleus	34

Figure 2A-C. Pearson correlation coefficients for the absolute grey matter (A), white matter (B), and cerebral spinal fluid (CSF) counts for all sub-volumes constructed using three different alignments to the population based target atlas: 12 parameter affine, 2nd order warp, and 6th order warp. All automated counts were compared against the "gold standard" native-space counts to produce "r values" across each of the twenty subjects used to construct the three sets of probability gradients. (See Table 1 for the regions studied).

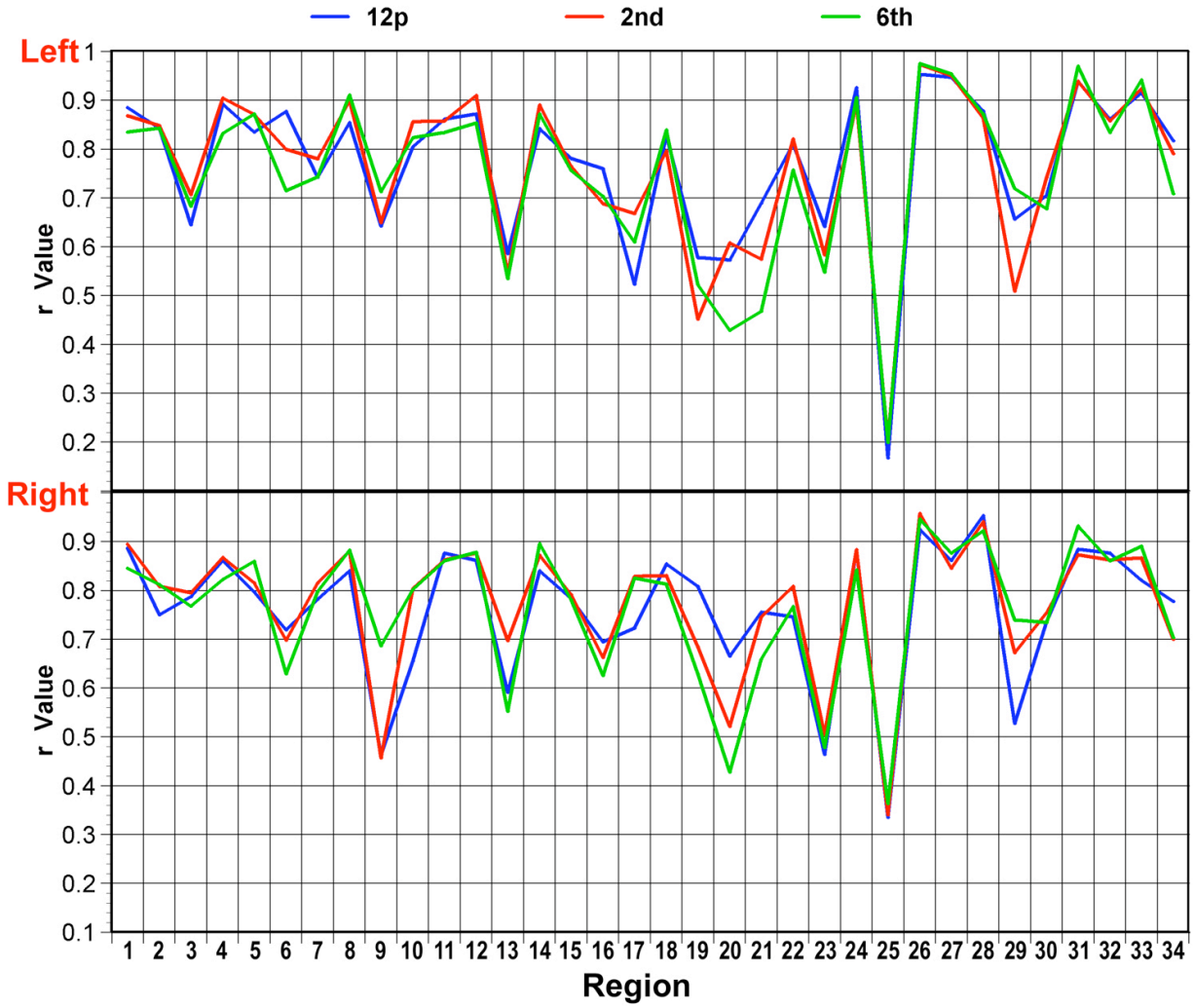

Figure 2B

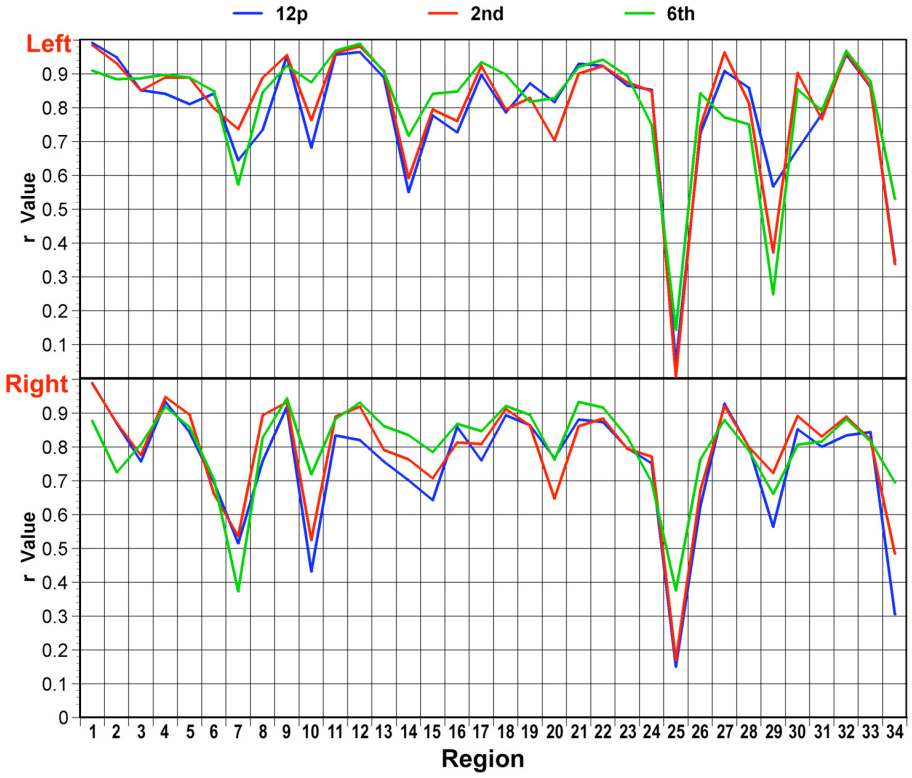

Figure 2C

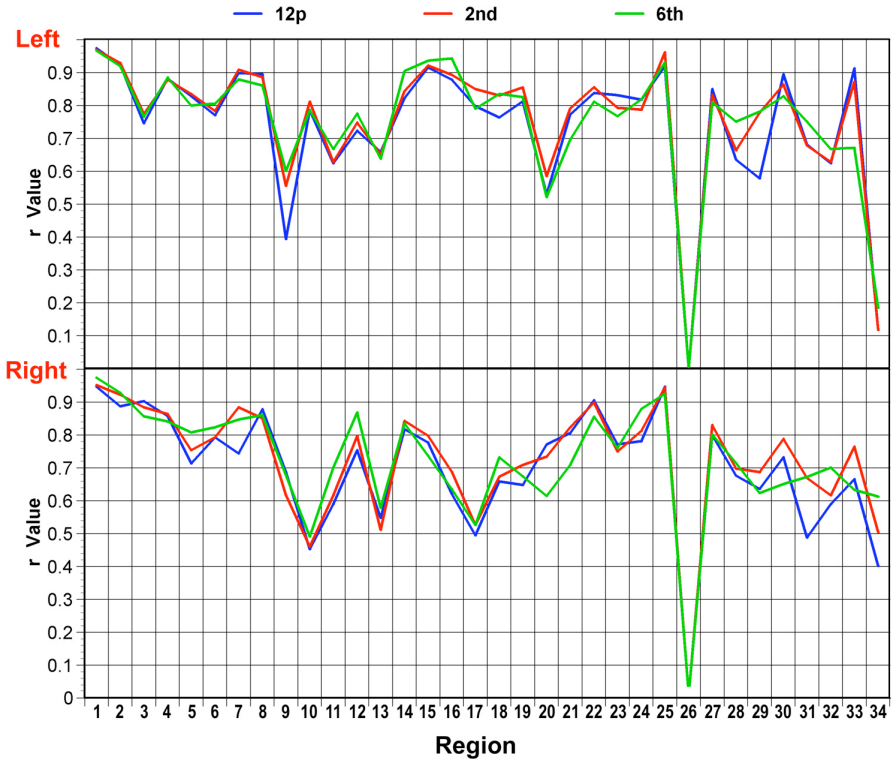

Figure 3AB. Pearson correlation coefficients for the grey matter (A) and white matter (B) ratios controlling for the amount of CSF in each sub-volume constructed (see text) using three different alignments to the population based target atlas: 12 parameter affine, 2nd order warp, and 6th order warp. All automated counts were compared against the "gold standard" native-space counts to produce "r values" across each of the twenty subjects used to construct the three sets of probability gradients. (See Table 1 for the regions studied).

Figure 3A

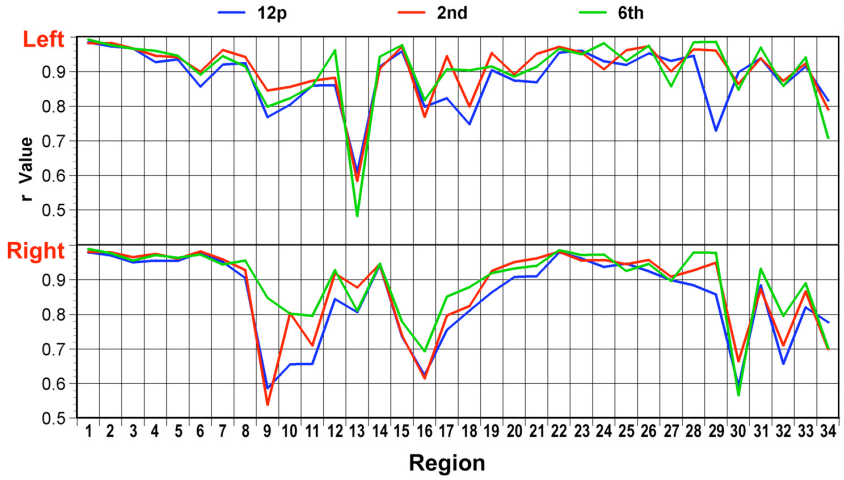

Figure 3B

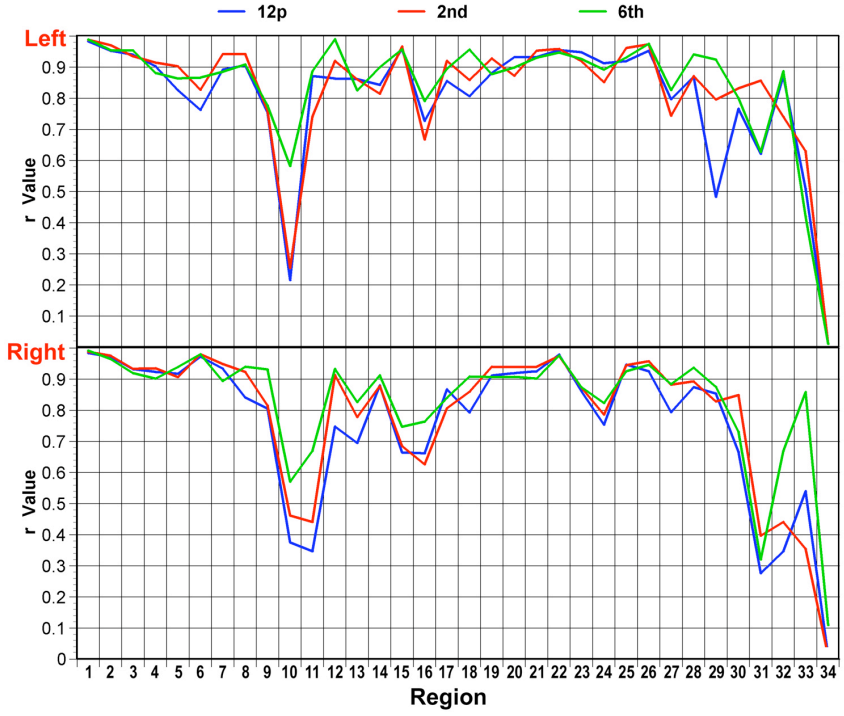

Note: absolute CSF counts used for the ventricles in A and B, absolute GM counts used for the hippocampus, thalamus, subtantia nigra, lenticular, and caudate nuclei in A.

Figure 4ABC. Probability gradients for grey matter voxels in medial temporal structures constructed across different registration matrices of the 20 subjects into the atlas. (A) Amygdalar gradients derived from 6th order warps (left) compared to 12 parameter registrations (right). (B and C) Hippocampal gradients derived from 6th order warps (left) compared to 12 parameter (right) registrations.

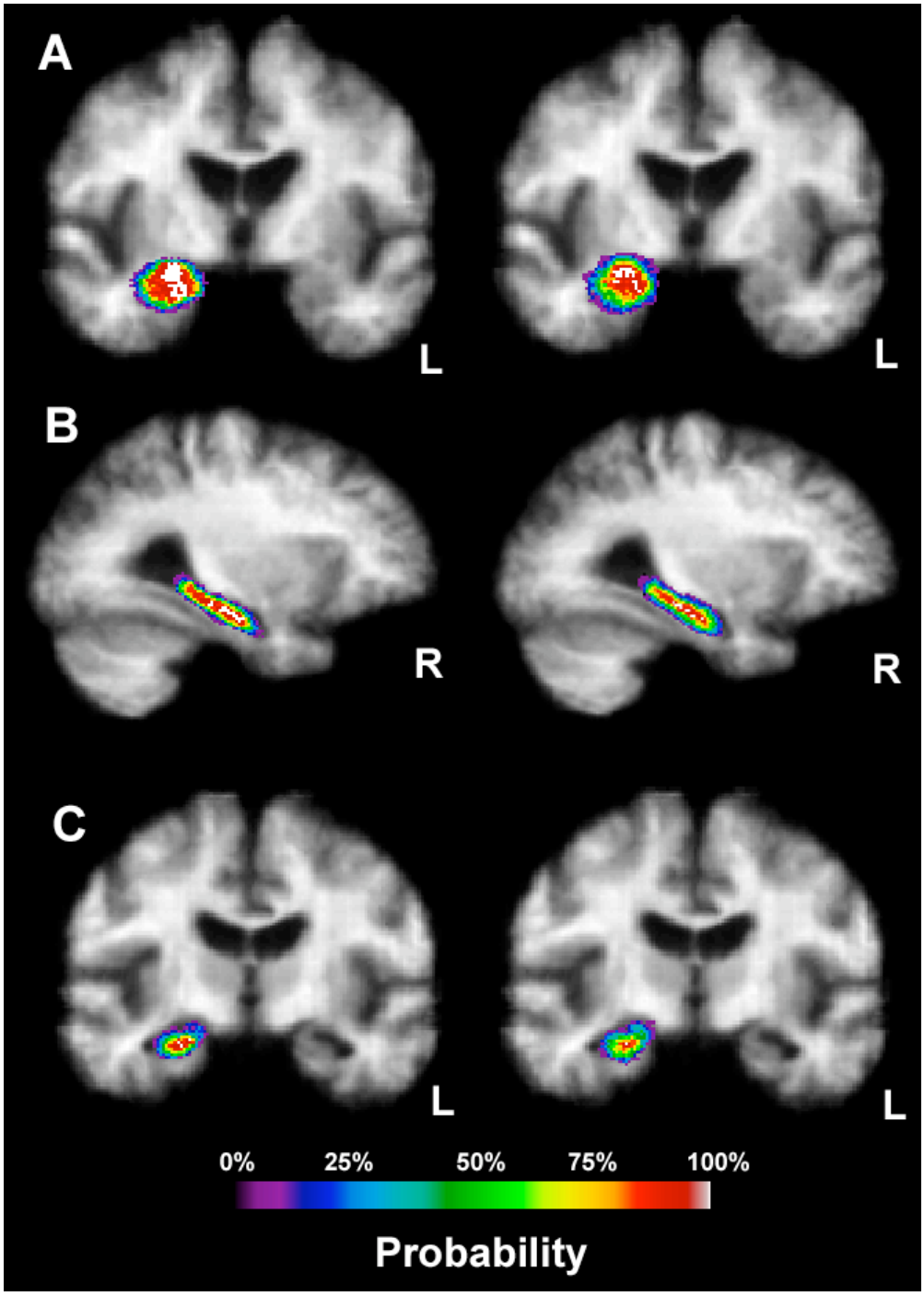

Figure 5ABC. Probability gradients for grey matter voxels in medial temporal structures constructed across different registration matrices of the 20 subjects into the atlas. (A) Anterior parahippocampal gradients derived from 6th order warps (left) compared to 2nd order warps (right). (B and C) Posterior parahippocampal gradients derived from 2nd order warps comparing the differential laterality effects in the population.

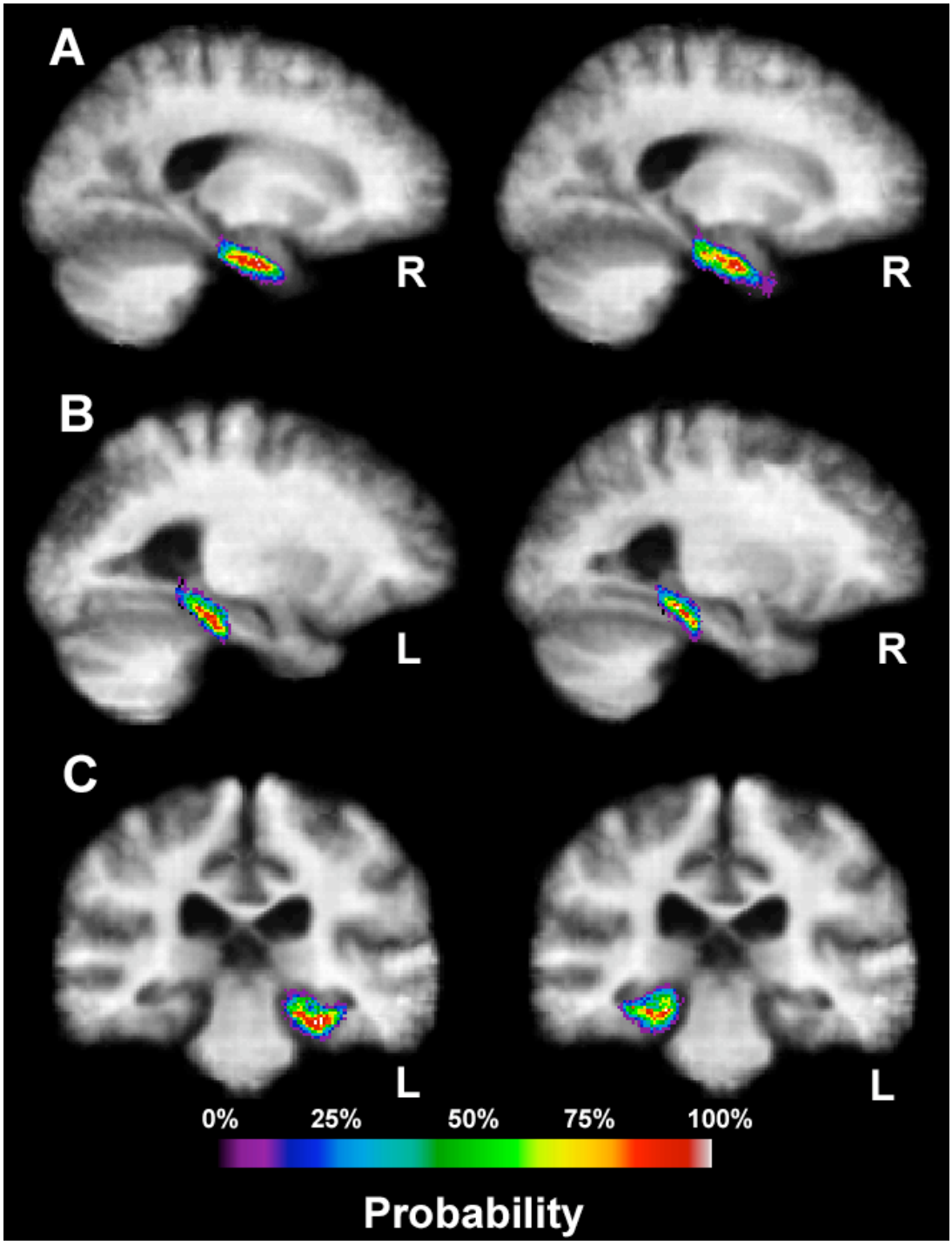

Figure 6ABC. Probability gradients for grey matter voxels in cortical structures constructed across different registration matrices of the 20 subjects into the atlas. (A) Lateral orbitofrontal gradients derived from 6th order warps (left) compared to 12 parameter registrations (right). (B) Subcallosal frontal gradients derived from12 parameter registrations comparing the differential laterality effects in the population.